Resources, Conservation & Recycling Advances 21 (2024) 200204

Contents lists available at ScienceDirect

Resources, Conservation & Recycling Advances

journal homepage: www.sciencedirect.com/journal/Resources-Conservation-and-Recycling-Advances

Utilization of high-volume fly ash in pervious concrete mixtures for mangrove conservation

Januarti Jaya Ekaputri [a,*], Xevna De Elshinta Arellsya Ruitan [b], Himawan Tri Bayu Murti Petrus [c], Martin Anda [d], Liliek Harmianto Purbawinasta [e], Irwanda Laory [f], Davin H.E. Setiamarga [g], Nobuhiro Chijiwa [h], Chikako Fujiyama [i]

[a] Civil Engineering Department, Institut Teknologi Sepuluh Nopember, Kampus ITS, Sukolilo, Surabaya, Indonesia
[b] Growth Center, Kompas Gramedia, Jalan Palmerah Barat, Jakarta, Indonesia
[c] Department of Chemical Engineering (Sustainable Mineral, Processing Research Group), Faculty of Engineering, Universitas Gadjah Mada, Jl. Grafika No.2, Kampus UGM, Yogyakarta, Indonesia
[d] Environmental Engineering, School of Engineering and Energy, College of Science, Technology, Engineering and Mathematics, Murdoch University, 90, South St, Murdoch, WA, 6150, Australia
[e] Environment VP, PT Petrokimia Gresik, Jl. Jend. Ahmad Yani, Gresik, Indonesia
[f] School of Engineering, The University of Warwick, Coventry, CV4 7AL, United Kingdom
[g] Department of Applied Chemistry and Biochemistry, National Institute of Technology (KOSEN), Wakayama College, Wakayama, Japan
[h] Department of Civil Engineering, Tokyo Institute of Technology, Japan
[i] Department of Urban Innovation, Yokohama National University, Tokiwadai, Hodogaya-ku, Yokohama, Japan

ARTICLE INFO

Keywords:
High-volume fly ash
Pervious concrete
Mangrove pot
Mixing sequence
Artificial aggregate

ABSTRACT

In environmental conservation, mangrove forests play a crucial role. Retransplanting mangrove propagules, however, faces challenges, and success rates are notably low. Achieving an optimal protector for propagules, balancing strength without impeding growth, is challenging. Mangrove propagules require a temporary protector with an optimal balance, neither too weak nor too strong, to shield them from current waves which is difficult. We propose using pervious concrete pots with high-volume fly ash activated with low NaOH concentrations. The investigation focuses on the influence of the mixing procedure on workability, compressive strength, and mineral composition. The novel discovery in this study is the specific sequence of stirring the ingredients using an alkali activator, which adds an interesting dimension to the research. It is recommended to adopt Sequence 2 in pervious concrete production, where NaOH dissolved FA in the mixture forming albite as N-A-S-H gel product. It surely enhanced both workability and the strength confirming uniform application processes. The two recommended variants, PFS-60 and PFBS-50, effectively utilize coal ash, meeting the target compressive strength range of 3–5 MPa and providing support for mangrove pots over a 3–4 year period. Notably, both compositions maintained consistent mechanical properties during exposure to tidal conditions for 240 days.They exhibit high permeability (694 liter/m^2/minute), facilitating efficient water passage without sediment entrainment.

1. Introduction

Mangrove forests offer a multitude of benefits, including coastal protection, prevention of sea water intrusion, and serving as habitats for diverse animal species (Stankovic et al., 2023). Protecting, managing, and restoring coastal blue carbon ecosystems can serve as a significant nature-based solution for addressing climate change (Montgomery et al., 2022). There has been a notable surge in global blue carbon research in recent decades, accompanied by substantial investments at national and international levels (Sievers et al., 2023; van Hespen et al., 2023). The preservation of these vital ecosystems is of paramount importance (Akram et al., 2023). Young mangroves are generally susceptible to barnacles, wave action, unsuitable soil conditions, and pollution. Various strategies have been employed to safeguard mangrove forests, such as planting mangrove saplings in coastal areas. As an example, in Indonesia, total mangrove critical land in 2019 was 637,624 Ha. The observed phenomenon led the government state to enact regulatory measures aimed at a grand design for mangrove rehabilitation efforts

* Corresponding author.
E-mail address: januarti@ce.its.ac.id (J.J. Ekaputri).

https://doi.org/10.1016/j.rcradv.2024.200204

Available online 8 February 2024

(Sabdaningsih et al., 2023). It was scheduled to be completed by the year 2024, encompassing a total land area of 600,000 Ha required 70 million USD. The total area of mangroves that have been rehabilitated from 2010 to 2021 is 118,970 hectares. However, mangrove saplings are susceptible to being easily swept away by waves. To address this challenge, affixing the saplings to logs or pipes has been attempted. Nevertheless, this approach exhibits a low success rate, especially in the face of larger waves, when sea-level rise has accelerated exponentially (Parkinson and Wdowinski, 2022). Hence, the development of alternative methods is imperative to shield mangrove saplings from the impact of waves while ensuring unimpeded plant growth for around 3–4 years after they are placed.

Some protection methods were applied to prevent mangrove propagules from swapping away during replantation. Nature-based coastal protection using rock fillets, fence from bamboos have proved generally successful to accumulate sediment for mangrove colonization (Morris et al., 2023; Strain et al., 2022). Nevertheless, while weak protection is unfavorable, overly strong protection is also not recommended. The saplings require more space to grow in multiple directions without restrictions.

On an alternative front, the Indonesian government has initiated a monumental project involving the construction of coal-fired power plants, boasting a collective capacity of 35 gigawatts, aimed at enhancing the electricity distribution network in Indonesia. The plants use coal as their fuel source for producing steam and are widely used for decades due to the abundance and relatively low cost of coal. This determined national project, however, presents a consequent challenge: a surge in coal waste production, specifically fly ash and bottom ash (FABA), arising from the combustion process (Darmansyah et al., 2023). This amplifies the incentive for international collaboration aimed at generating innovative strategies for maximizing coal utilization. Furthermore, it is widely recognized that fly ash (FA) holds substantial promise as a viable constituent material within concrete formulations.

The high-volume fly ash (HVFA) technique, which integrates FA as a cement substitute at levels reaching or more than 50 % by binder mass, emerges as a viable solution for mitigating the proliferation of FA. When incorporated into self-compacting concrete, formulations utilizing up to 80 % FA exhibit elevated absorption rates compared to conventional concrete, coupled with diminished shrinkage, especially in comparison to counterparts incorporating 20 % or 30 % FA by weight (Laxman Kudva et al., 2022; Promsawat et al., 2020). However, HVFA applications exceeding 70 % as a cement substitute are best suited for concrete mixtures with lower compressive strength targets (Aydin and Arel, 2017). To improve the strength of concrete, mixing fly ash with alkali activator in low concentration increases the solubility of coal ash (Wilińska, 2023).

Bottom ash (BA), characterized by its porous particle structure, mitigates concrete shrinkage while displaying high water absorbability and irregular particle morphology (Rafieizonooz et al., 2016). Its extensive replacement of sand is discouraged in high-workability concrete mixes. Nonetheless, it finds applicability in paving mixtures, hollow blocks, and other products where high workability is not a primary requirement (Singh and Siddique, 2016). The addition of 10 % ground BA as a supplementary cementitious material in concrete mixtures imparts notable effects on weight variations, compressive strength, and chloride penetration. Concrete subjected to chloride attack, fortified with BA, exhibits a remarkable reduction ranging from 42 % to 45 % at 180 days compared to conventional concrete (Mangi et al., 2019).

FABA emerges as a versatile component, finding utility in various concrete types, including pervious concrete. The integration of artificial aggregates derived from FA into pervious concrete formulations imparts lightweight properties, thereby reducing the overall weight of the concrete structure (Rupesh et al., 2015; Sherwani et al., 2021). These lightweight artificial aggregates, while demonstrating higher porosity and water absorption, exhibit diminished compressive strength in contrast to their natural counterparts (Shanmugan et al., 2020; Ul Rehman et al., 2020)

This study's objective is to maximize the utilization of FA in substantial volumes. Additionally, the investigation explored the application of pervious concrete, incorporating artificial aggregates derived from FA, as a provisional container to safeguard mangrove saplings during their initial growth stages. Pervious concrete, distinguished by its minute pores, allows seawater to permeate, rendering it more convenient for usage in this context compared to solid concrete structures that necessitate accurate hole creation (Tuan et al., 2022). The envisaged pot required adequate strength to sustain its own weight, support the enclosed plantation, and withstand wave forces until the saplings matured enough to establish firm roots. However, an excess of strength was undesirable; instead, the pot was designed to self-degrade progressively as the saplings developed their root systems. Consequently, the target compressive strength for the pervious concrete was set at approximately 3–5 MPa, a value determined through rigorous considerations of various external and internal pressures acting upon the pot. To fulfill these criteria, the study systematically investigated the optimal composition for pervious concrete, employing FABA as a binder and artificial aggregate. FA incorporation reduces concrete's carbon footprint by decreasing cement content, curbing CO_2 emissions, especially in mangrove conservation efforts (Cooke et al., 2020).

This study proposes not only the material proportions to produce pervious concrete using artificial aggregate with alkali to activate HVFA, but also recommends the mixing sequences with alkali for the paste. The artificial aggregate was entirely utilized, serving as a 100 % substitute for natural aggregate, and was shaped into small spheres with a maximum diameter of 20 mm. The paste in pervious concrete formulations utilized a HVFA binder, incorporating FA content ranging from 50 % to 70 % of the cement's weight. Additionally, one of the mixtures incorporated BA. To augment the strength of the composite, rice husk was introduced as a natural reinforcing element at a concentration of 1 % relative to the total weight of the binder. Rice husk was specifically chosen as the natural fiber due to its advantageous tensile strength characteristics, which effectively mitigate cracking during the concrete's placement (Chen et al., 2023; Li et al., 2021; Liu et al., 2023). However, it is important to note that rice husk is susceptible to degradation over time when exposed to prolonged marine conditions (Liu et al., 2022). Despite this vulnerability, the use of rice husk as a short fiber reinforcement was favored due to its capacity to enhance the composite's strength without compromising concrete workability in comparison to longer fibers.

2. Mangrove pot concept

2.1. Pot design

Various initiatives aimed at ensuring the success of mangrove planting involve implementing protective barriers for seedlings to shield them against wave impacts. Ideally, planted mangroves exhibit a diverse range of species (Sam et al., 2023). Consequently, sediment availability in mangrove areas is of paramount importance, serving as a crucial medium for anchoring the roots of mangrove vegetation. Projects utilizing bamboo for protection often demonstrate limited effectiveness due to the material's lack of durability and susceptibility to damage in aggressive environmental conditions (Nguyen et al., 2017). In contrast, the method involving the deployment of wave-blocking stones is specifically designed to accumulate sediment, fostering optimal conditions for the growth of mangrove saplings. Nevertheless, this approach necessitates the deployment of substantial and sizable rock piles, potentially posing interference with the uniform growth of mangroves.

In general, *Rhizophora mucronata* stands out as the preferred species for transplantation to control erosion due to its local adaptability and ease of transplantation. Effective mangrove planting strategies, demonstrated by the Indian government in Gujarat, encompass three methods: direct seed planting, the fishbone pattern, and elevated

planting beds (Shah and Ramesh, 2022). The latter method proves most efficacious in regions prone to high tidal waves. In such instances, optimizing sediment accumulation and mitigating ocean currents through the deployment of temporary barriers are considered the most favorable approaches.

This study has encouraged efforts to utilize porous concrete as a temporary container for safeguarding mangrove saplings. The selection of pervious concrete for mangrove pots was based on its optimal performance in terms of mechanical strength, hydraulic resistance, meeting structural requirements, sustainability, and achieving the necessary durability (Adamu et al., 2021). By modifying pervious concrete with fly ash, neither the void ratio nor the permeability have been negatively affected by improving the strength of the material (Adresi et al., 2023).

It features interconnected holes and pores (2–8 mm) for effective drainage. Desired porosity is achieved using uniform granular-shape aggregates (19–9.5 mm), without fine aggregate, distinguishing it from conventional concrete, which has a range of aggregate sizes. Pervious concrete's large pores allow easy water and air passage, a contrast to conventional concrete. Porous concrete has various applications such as pavements, walls, thermal insulation, coastal structures, and low-strength airport surface.

The durability of pervious concrete for mangrove pot is very important as it serves both mechanical and environmental load in seawater. It is influenced by mix design, aggregate type and size, workability, binder type, and operational aspects. To optimize mix design, this study examines these factors with a focus on FA application and mixing procedures.

The selection of high-volume FA material was motivated by the concerns encompassing the material's durability in marine environment. The design objectives require that the container must exhibit adequate strength to endure three primary stress factors: its own weight, the planting substrate within it, and the force exerted by oceanic waves. This durability is necessary for a constrained duration of three years, until the mangrove roots have sufficiently developed to provide autonomous support. Nevertheless, the pot should not be excessively strong to accommodate the anticipated growth of the mangrove roots. Furthermore, the design must facilitate unimpeded water circulation into the pot while preventing sediment egress. Porous concrete was selected as the ideal material, as it can satisfy these requisites and is more manageable than perforated solid concrete pots, as depicted in Fig. 1.

The achievement of an average growth percentage exceeding 50 % in mangrove plants can be considered successful, given the inherent challenges associated with mangrove cultivation. This success threshold is particularly relevant for pure planting schemes employing spacing configurations of 2 × 1 m and 1 × 1 m, accompanied by seed densities of 5000 and 10,000 seedlings per hectare, respectively. Conversely, for mangrove plants planted at 1 × 3 m and a seed density of 3000 seeds per hectare, the minimum plant growth percentage reaches 70 %. The attainment of a three-year survival milestone signifies the plant's strength and bodes well for its continued maturation, provided it remains unimpeded by external disturbances such as fire, logging, or encroachment for alternative purposes, such as aquaculture.

Cylindrical concrete containers can be conveniently fabricated on land and subsequently transported to the mangrove planting site for assembly. This size has been carefully engineered to enhance the success rate of mangrove planting until its roots growth safely inside the pot, aligning with the most suitable spacing parameters as shown in Fig 2**(a)**. To mitigate the impact of wave energy, pot-shaped breakwaters are strategically deployed as protective barriers in the vicinity, affording additional defense for the planted mangroves. In Fig. 2**(b)**, an arrangement of mangrove-containing pots is illustrated, positioned in tandem with an array of perforated pots serving as wave-breaking barriers. These protective structures not only act as a shield against the impact of large waves but also serve as sediment collectors, contributing to the overall stability of the mangrove-containing pots. The sediment accumulation plays a pivotal role in enhancing the structural integrity of the mangrove pots, mitigating the risk of overturning induced by prevailing currents and tidal flows.

2.2. Calculation for internal and external pressure of pervious concrete pot

Two distinct types of pressure model influence the pervious concrete pot: internal and external pressure. Internal pressure arises from saturated sediment trapped inside the pot when water levels are low, leading to stresses within the pot, as depicted in Fig. 3.

The horizontal stress resulting from sediment pressure at the base of the pot, σ_H, is determined by the combined effects of horizontal stress due to active sediment pressure and water pressure when the sediment is in a saturated state within the pot. We asumed a sediment cohesion (C) value of 0.03 kN/m^2 with dry densitiy of sediment of 17.28 kN/m^3 and a friction angle of 3.5° for depths up to 4 m, as reported by previous study (Faturachman and Raharjo, 2003). Considering a Rankine coefficient of 0.88 for active earth pressure with density of sea water is 1.03 ton/m^3, the horizontal stress attributable to sediment pressure (σ_{Hs}) within the pot is represented by Eq. (1). The pressure exerted by deep-sea water (σ_{Hw}) within the pot, containing saturated sediment, is expressed through Eq. (2).

$$\sigma_{Hs} = (\gamma_{\text{sediment}} \times H)K_a - 2 \times C \times \sqrt{K_a} \quad (1)$$

$$\sigma_{Hw} = (\gamma_{\text{seawater}} \times H) \quad (2)$$

In cylindrical pressure vessels, radial stress, longitudinal, and stress lateral stress are essential components that influence stress distribution. These stresses are vital considerations in the design and analysis of pressure vessels to ensure their structural integrity and safety under various operating conditions.

In this study, the specific stresses within the pervious concrete pot were analyzed, focusing on radial stress (σ_1), longitudinal stress (σ_2), and lateral stress (σ_3), as ilustrated in Fig. 4.

The stress (σ_3) is equal to total horizontal internal pressure σ_H, quantified as 0.01 MPa, contributed from Eqs. (1) and (2).

Fig. 1. Design of mangrove pot from pervious concrete.

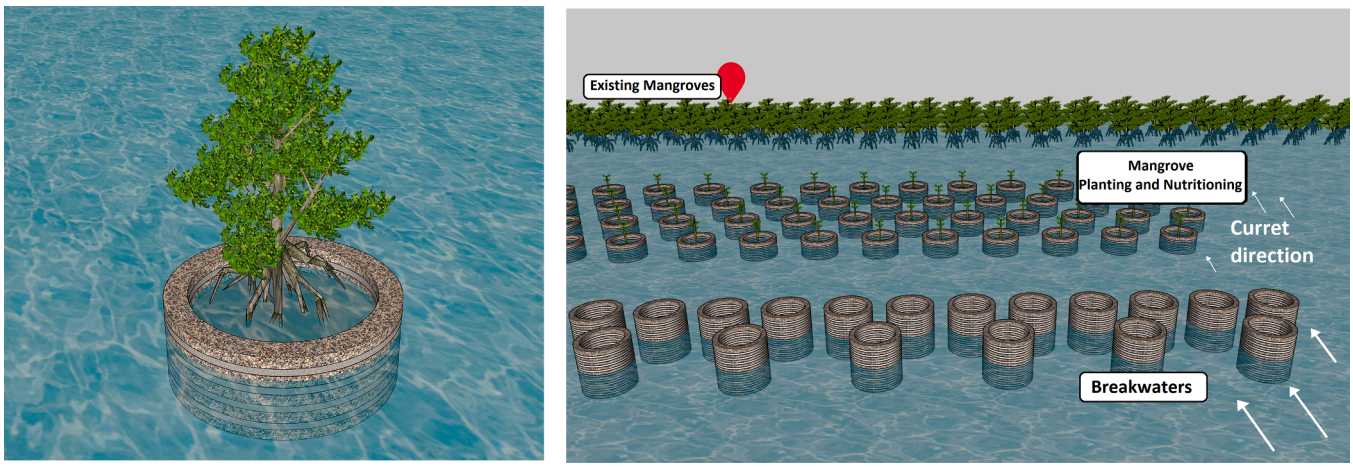

Fig. 2. Pervious pot for saplings protection.

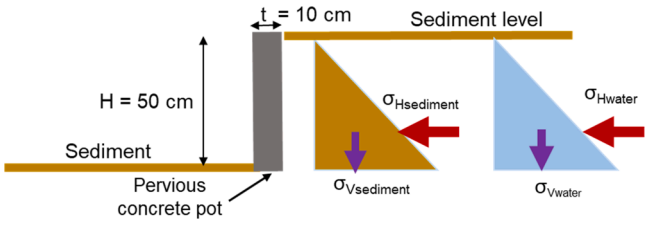

Fig. 3. Internal stress from saturated sediment.

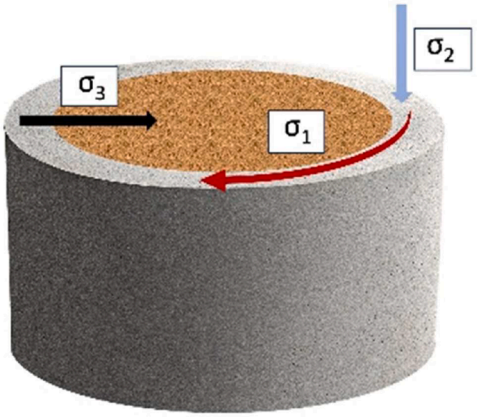

Fig. 4. Stresses within cylindrical pervious concrete pot.

Radial stress (σ_1) occurs tangentially along the circumference of the vessel's cross-section. It is caused by the internal pressure acting on the vessel's walls with a radius (r) of 0.4 m and thikness (t) of 10 cm. It is calculated using Eq. (3).

$$\sigma_1 = \frac{\sigma_3 \times r}{t} \tag{3}$$

Longitudinal stress (σ_2), runs along the length of the vessel and is also caused by the internal pressure. It is calculated using Eq. (4).

$$\sigma_2 = \frac{\sigma_3 \times r}{2t} \tag{4}$$

Radial stress (σ_1), longitudinal stress (σ_2), and lateral stress (σ_3), were quantified at magnitudes of 0.04 MPa, 0.02 MPa, and 0.01 MPa, respectively. Consequently, the pot was required to possess a minimum tensile strength of 0.04 MPa to effectively withstand these stresses, ensuring its structural integrity under the anticipated internal and external pressure conditions. This detailed stress analysis provides valuable insights into the material's mechanical behavior and aids in the precise design and evaluation of pervious concrete pot structures for protecting mangrove sapplings.

External pressure, originating from wave forces outside the pot, acts in support of the pot, helping it endure internal forces, as illustrated in Fig. 5. The pressure represents the dynamic pressure exerted by sea waves on a structure's surface (Takagi, 2023). It is important to note that many propose equations provide an approximation and might not cover all the complexities of real-world wave interactions with structures.

The pressure caused by waves (P) outside the pot is calculated using Eq. (5) and Eq. (6).

$$P = \gamma_{\text{seawater}}\, g\, \eta \tag{5}$$

$$\eta = 0.75\,(1+\cos\beta)\lambda H_D \tag{6}$$

where:

P = sea wave pressure (kN/m^2)
γ_{seawater} = at a temperature of 0 °C and an atmospheric pressure of 1 atm = 1.03 t/m^3
g = Gravitational acceleration
η = height above the original water level (m)
β = angle between the normal line and the direction the wave comes from
λ = wave pressure modification factor (standard value = 1)
H_D = wave height (m)

In the calculations, it is assumed that the incoming waves approach the pot perpendicularly, and the selected wave height corresponds to the

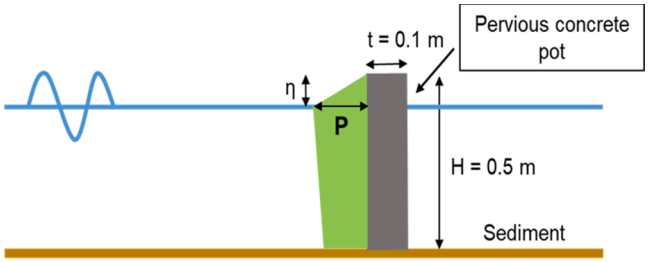

Fig. 5. Pressure from wave force.

intended pot height of 0.5 m, as depicted in Fig. 5. From these calculations, the following results are obtained: the wave peak elevation (η) is estimated to be 1.125 m, and the corresponding wave pressure (P) is calculated to be 1.159 kN/m^2 that is much lower than the internal force inside the pot. However, this external pressure from the waves can act as an active counterforce to prevent abrupt structural failure, such as splitting, that can occur due to internal forces within the pot.

3. Materials and methods

3.1. Materials

In this investigation, FABA utilized in Fig. 6 were sourced from pulverized coal combustion (PCC) boiler in PT Petrokimia, Gresik, Indonesia. The characterization of toxic components and chemical composition within the FABA samples was conducted through X-ray fluorescence (XRF) test and toxicity characteristic leaching procedure test (TCLP). Particles of FABA analyzed using Scanning Electron Microscopy (SEM), are depicted in Fig. 7. The examination of FA illustrates the existence of small spherical particles, distinguished by their rounded shape. Its particles exhibited a weight passing rate of 82.6 % through sieve no. 325. Meanwhile, BA exhibits irregular particle shapes that are larger than FA, and its particles appear porous.

Chemical analysis for the FABA with X-ray fluorescence (XRF) is presented in Table 1. The FA exhibits elemental composition, with SiO_2, Al_2O_3, and Fe_2O_3 each surpassing the 50 % threshold, while CaO content remained below 18 %. In accordance with the classification specified in ASTM (C618, 2019), it is classified as class F.

The silica present in FA is not entirely soluble and reacts with the byproducts of cement hydration. Gravimetric testing revealed that only 69.4 % of the silica in FA is reactive. Furthermore, the pozzolanicity of FA was assessed using the strength activity index (SAI) with Portland cement at 28 days according to the ASTM (C595, 2020) Annex 1. FA Petrokimia demonstrated a strength activity index of 79 %, surpassing the minimum requirement of 75 %.

The results of TCLP of FABA according to Indonesian government regulation is presented in Table 2. The test is important to assess potential risks to human health and the environment. These results play a crucial role in ensuring the safety of material applications in adherence to regulatory standards.

Importantly, the toxic content within this FABA sample adhered to the safety standards delineated in the Regulation of Government of Republic of Indonesia (PP.22/2021), as indicated by the TCLP results. The study's findings indicate that all ash materials examined are below the hazardous substance dissolution standard set by the regulation for TCLP. Consequently, FABA meet regulatory standards and qualify as suitable byproduct materials. The significance of TCLP results extends beyond Indonesia, as other countries also uphold strict regulations for FABA applications (Lo et al., 2021). Ecological assurance can be established as FABA collected from PCC boilers qualifies as inert waste that contained minimal leaching of heavy metals (Arenas et al., 2015; Gupta et al., 2019). In addition, it can be effectively utilized as a substitute or alternative material in marine applications (Lee et al., 2016; Park et al., 2009). Consequently, it is unlikely to pose any hazard to public health and the environment.

Fig. 6. Fly ash (left) and bottom ash (right).

In addition, the density measurements for FA, BA, and Portland Cement were recorded at 2.46 g/cm^3, 2.17 g/cm^3, and 2.97 g/cm^3, respectively, providing essential physical property data that contributes to the comprehensive characterization of these materials for various scientific and industrial applications.

Two types of liquids were employed in the study: water and a 0.03 M sodium hydroxide (NaOH) solution. The choice of activator significantly influenced the resultant mechanical properties, a factor critical in this study's background. The selection of solvent for preparing paste, both for artificial aggregate and pervious concrete, was NaOH 0.03 M solution. Low-alkalinity activator was desired due to its profound impact on mechanical characteristics, a point well-established in literature (Wu et al., 2024). It was imperative to note that varying solvents could potentially influence compressive strength, a vital parameter in concrete performance (Palomo et al., 2007). It increases the pozzolanic reaction as an initiation of dissolved of FA.

During the concrete mixing process, rice husk, sourced was incorporated as a natural fiber. The uniform distribution of the fibers played a crucial role in enhancing early strength (Singh, 2021), a property pivotal in the context of this study. It was important to acknowledge that it aided in mitigating shattering, it concurrently led to reductions in compressive strength and splitting tensile strength (Akturk et al., 2016). Moreover, rice husk possessed high absorption characteristics, which posed challenges to concrete workability (Chabi et al., 2018). Consequently, adding rice husk beyond 1.5 % and other natural fiber more than 5 % led to significant declines in both compressive strength and workability (Lawala et al., 2019; Tijani et al., 2022). Thus, an optimal ratio of 1 % of rice husk from the binder's weight was determined to strike a balance between reinforcing the concrete structure and maintaining workability. The sediment employed in the permeability tests was sourced from the mangrove eco-tourism area in Wonorejo, Surabaya, Indonesia.

3.2. Mixing sequence procedure

The mixing sequence procedure in concrete production involves a systematic order of adding and blending ingredients to achieve a homogeneous, workable mixture, and better mechanical properties. Workability is a crucial requirement for formulating the binder in porous concrete mixing (Vieira et al., 2020) as it increases the tensile of concrete (Gupta et al., 2021; Salas_Montoya et al., 2023). In the absence of fine aggregate, the binder must connect granular aggregate with a very thin layer to prevent excessive paste coverage over the holes. Maintaining an optimal water-to-cement (w/c) ratio is essential; high water content weakens the bond between aggregates, while a low w/c ratio reduces workability and may close the preferable holes in the concrete structure.

The replacement of cement with FA led to a decrease in the mixture's pH, resulting in a slower activation of FA. Maintaining a pH range of 12.3–12.5 is considered the optimal condition for pastes containing very high-volume FA (Pratiwi et al., 2017, 2020). A 0.03 M sodium hydroxide (NaOH) solution was utilized to enhance the solubility of FA. Other option is applying liquid activators as water replacement such as calcium sulfate, sodium sulfate, calcium hydroxide (Luo et al., 2024; Qi et al., 2023; Wilińska, 2023) .

The mixing sequence involving alkali in the production of HVFA paste is a novel approach. Past studies have suggested the use of alkaline solutions in the mix, but specific recommendations regarding the sequential order of ingredient mixing were lacking. In this study, five different sequences were employed to assess the impact of various mixing sequences on the properties of the resulting HVFA-based materials. We employed a 0.03 M NaOH solution as the activator, replacing

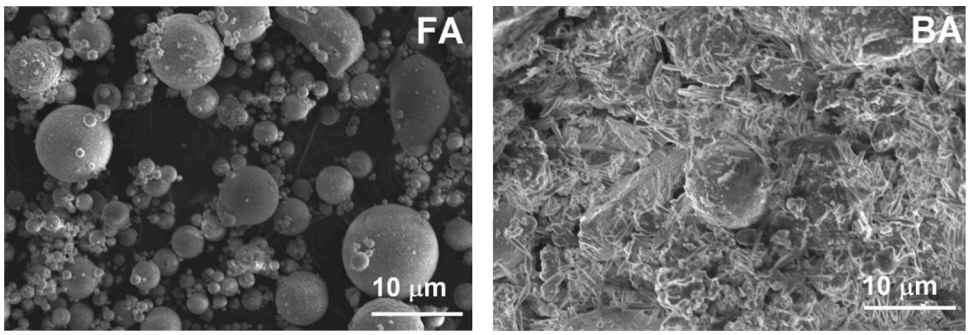

Fig. 7. SEM analysis at 2500× magnification for FA (left) and BA (right).

Table 1
Chemical composition in FA and BA (% mass).

Material	SiO_2	Al_2O_3	Fe_2O_3	CaO	MgO	Na_2O	K_2O	TiO_2	MnO_2	Cr_2O_3	P_2O_5	SO_3
FA	47.82	18.40	18.84	6.80	2.42	0.78	1.48	0.86	0.30	0.01	0.34	1.50
BA	57.87	13.59	15.92	5.12	1.77	0.48	0.90	0.68	0.18	0.02	0.65	2.38

Table 2
Toxic content in FABA (mg/L).

Material	Cd	Cr^{6+}	Cu	Pb	Ag	Zn	B	CN^-	F	NO_3	NO_2
FA	0.03	0.03	0.11	0.26	0.03	0.03	6.24	0	12.16	28.67	4.02
BA	0.06	0.06	0.19	0.02	0.02	0.05	5.94	0	10.82	42.01	5.08
Indonesia EPA regulation level (max)	0.15	2.50	10.00	0.50	5.00	50.00	25.00	3.50	75.00	2500	150

either all water or only 50 % of the water in the process. Liquid (water and/or alkali) to binder ratio was kept at 30 % for all sequences. In every sequence, all mixtures were stirred for 20 rounds. These sequences were systematically designed to explore the distinction effects of varying mixing orders on the resulting materials' properties, providing valuable insights into their structural and mechanical characteristics. The five sequences are as follows:

- **Sequence 1** start with blending dry FA and portland cement, followed by the addition of water and uniform stirring.
- **Sequence 2** involved the combination of dry FA and portland cement, followed by the introduction of NaOH 0.03 M solution, equivalent to the water quantity used in Sequence 1, and further stirring.
- **Sequence 3** initiated with dividing the total liquid weight into two equal parts. Half constitutes water, while the remaining portion is composed of NaOH solution. The total volume of NaOH 0.03 M solution was a half of liquid quantity used in Sequence 1. Then, mixing the FA with NaOH 0.03 M solution for 10 min, followed by the addition of portland cement and water to the FA slurry.
- **Sequence 4** commenced with the combination of FA with NaOH 0.03 M solution for 10 min, followed by the addition of portland cement and stirring. The total volume of NaOH 0.03 M solution matched the total water quantity used in Sequence 1.
- **Sequence 5** involved the initial mixing of FA with NaOH 0.03 M solution (half of total liquid) for 10 rounds, followed by the water to the FA slurry and stirring for another 10 rounds. Subsequently, portland cement was added, and the mixture was stirred for an additional 20 rounds. The total volume of NaOH 0.03 M solution and water equaled that used in Sequence 4.

For sample with 50 %FA (AFS-50), the paste was made by following sequence 1–5 to analyze the effect of different mixing sequence on the workability. Sample AFS-50 was tested for its mineral content, paste workability, and compressive strength. Mineral content was obtained from XRD test. Workability was tested by using normal consistency of hydraulic cement paste method from ASTM (C187, 2016) to analyze the penetration of vicat needle of each paste with different sequence. This test provides information of required water for the paste. Sample containing 40 %FA (AFS-40) and 60 %FA (AFS-60) were only tested for its compressive strength. The test was conducted in the age of 28 days for cylindrical specimens with a diameter of 2 cm and a height of 4 cm. An average strength was analysed from selected six identical pastes. The optimal FA content and paste's compressive strength variation were used as a basic for artificial aggregates. The sequence that show the optimum result on the paste workability, minerals content, and compressive strength were used to produce the binder of pervious concrete

3.3. Production of artificial aggregates

The pervious concrete was produced by using uniformly graded granular aggregates with diameters ranging from 4.75 mm-9.5 mm and diameters from 9.5 to 19.0 mm to achieve adequate permeability. Some trials were conducted to find the optimum variation to produce artificial aggregates. The paste with FA content 40 %, 50 %, and 60 % was made. The best performance from these mixture was selected for pervious concrete production. The proportions are presented in Table 3.

In this method, cement and FA, in dry powder form, were initially mixed at room temperature and then added to the flat pan of a granulator machine. The granulation process, lasting approximately 30–40 min, involved continuous rotation of the pan. During the initial 2–3 min, a NaOH solution was sprayed onto the powder surface using a sprayer

Table 3
Artificial aggregate compositions.

Sample	FA (%)	PCC (%)
AFS-40	40	60
AFS-50	50	50
AFS-60	60	40

while the granulator continued to rotate. The quantity of liquid sprayed was estimated to be 30 % of the powder mass. The pan continued to rotate to form the spherical fresh aggregate. After the granular aggregates were form, FA was added to the surce of aggregates to prevent the ballsformedached each other when the exessive liquid might unite the fresh aggregates. The aggregates were cured in moist condition for 28 days before utilizing to produce pervious concrete. Subsequent to their production, the physical properties of these artificial aggregates were methodically evaluated through a series of tests encompassing density, absorption, porosity, and abrasion analysis.

The artificial aggregates depicted in Fig. 8 were generated with a granulator pan, the slope of which was precisely set at 50°, as depicted in Fig. 9. This specific slope angle was selected due to its proven efficiency in yielding aggregates with the lowest absorption rate when compared to slopes of 45° and 55°. It also had less unfinished ash particles which should react with the alkaline solution (Yuliana et al., 2019).

Porosity testing adheres to the guidelines outlined in ASTM (C642, 2013). The test results provide the open pore volume. Calculation of the total pore volume involves grinding the sample and measuring its volume, accounting for both open and closed pore volumes as formulated in Eqs. (7) to (9). The total pore volume is then interpreted as the combined sum of the open pore volume and the closed pore volume, where g_1 represents the bulk density in dry condition (g/m^3), g_2 is the apparent density (g/m^3), and g_3 is the absolute density (g/m^3).

$$Open\ porosity = \left[\frac{g_2 - g_1}{g_2}\right] \times 100 \tag{7}$$

$$Total\ porosity = \left[\frac{g_3 - g_1}{g_3}\right] \times 100\% \tag{8}$$

$$Closed\ porosity = Total\ porosity - Open\ porosity \tag{9}$$

It is essential to note that accurately determining the specific gravity of these artificial aggregates posed a challenge. This difficulty arose from the inherent complexities associated with ascertaining the saturated surface dry (SSD) condition of artificial aggregates (E1-16, 2016). These aggregates tend to absorb water rapidly, rendering them relatively heavier when in the SSD state. To address this, the soaked aggregates were left to air dry for a duration of 15 to 20 min, allowing them to reach a visually dry state. Both the paste and artificial aggregates were subjected to a moist curing process to ensure their optimal properties and performance.

3.4. Pervious concrete casting

Pervious concrete was prepared by using only two size gradation of artificial aggregates, without sand. Weight ratio of 4.75 - 9.5 mm and 9.5–19 mm aggregates were 1:1.5 respectively. The mixture were proportioned based on a recommendation on pervious concrete (ACI, 2010). After trial and error, mix design of pervious concrete was obtained which is listed in Table 4. Sequence 2 was selected as the casting method because of its strength and great workability. The motivation of this study to apply HVFA as the binder is for using maximum cement in the range of 30−40 % from total binder. Therefore, the variation of FA in binder are 50 %, 60 %, and 70 % by cement's weight. Furthermore, BA was also added into PFBS-50 variation to replace 10 % cement weight considering its contribution to against chloride attack in seawater environment. Variation with BA and higher FA content (PFBS-50 and PFS-70) required higher water content than FPS-60.

Fig. 8. Artificial aggregates.

Pervious concrete was casted into cylinder and slab specimens. Despite its significant durability performance in seawater (Mangi et al., 2019), the substitution of cement with BA should not exceed 20 %, as it leads to a decrease both workability and the tensile strength (Al Biajawi et al., 2022; Tamanna et al., 2023).

Cylinder specimens were caped using AFS-60 paste at least 1 cm thick on top and bottom of the cylinder. The diameter of specimens of 10 cm and height of 20 cm as presented in Fig 10**(a).** The slab was made which is presented in Fig. 10**(b)**. Cylinder specimens were prepared for the compressive strength test, while slab specimens having a size of 30 × 30 × 10 cm were made for the permeability test as presented in Fig. 10**(c)**. Three identical slab specimens were analyzed for the average strength.

The trial tests revealed that the aggregates exhibited a notably high rate of porosity and absorption, factors demanding careful consideration during the material mixing process. To mitigate the rapid absorption of the solvent by the aggregates before their reaction with the binder, a specific mixing sequence was adopted. Initially, the binder pastes were thoroughly mixed, followed by the gradual addition of aggregates and rice husk. This sequential addition strategy aimed to prevent premature solvent absorption, ensuring an efficient chemical reaction between the aggregates and the binder components. Subsequently, four identical cylinder specimens were prepared and subjected to testing at the ages of 28 and 56 days to assess their mechanical properties and durability. Notably, all pervious concrete specimens submitted to careful moist curing procedures, a vital step in ensuring the optimal development of their structural integrity and performance characteristics. Furthermore, to obtain the effect of seawater environment on the compressive strength, cylindrical specimens undergone curing for eight months at in tidal area near mangrove forest, Surabaya, Indonesia.

Additionally, it is observable that the cement adheres to the structure of the plant used for reinforcement as presented in Fig. 11 with 25× magnification. This cohesive interaction contributes to the strength and lightweight characteristics of the composite. The effective penetration of cement into the deeper recesses of the rice husks indicates strong adhesion between the cement material and the plant fibers (Doumongue et al., 2023).

3.5. Water and sediment permeability

Water permeability test was conducted to determine how long one liter of water took to seep through pervious concrete per m^2 area that is illustrated in Fig. 12.

The measurement was expressed as volume per unit area per unit time, calculated using Eq. (10).

$$\text{Water Permeability} = \frac{V \times 60}{t \times A_{Slab}} \tag{10}$$

The surface area, A_{Slab}, serves as a crucial parameter (m^2), providing the geometric context for the permeation process. Time, denoted by t, is a key metric representing the duration (minute) taken for water to infiltrate the material, indicating its permeability rate. Lastly, the volume of water (V), expressed in liters, quantifies the amount of liquid involved in the permeation test, offering valuable insights into the material's absorptive capacity and behavior under specific environmental

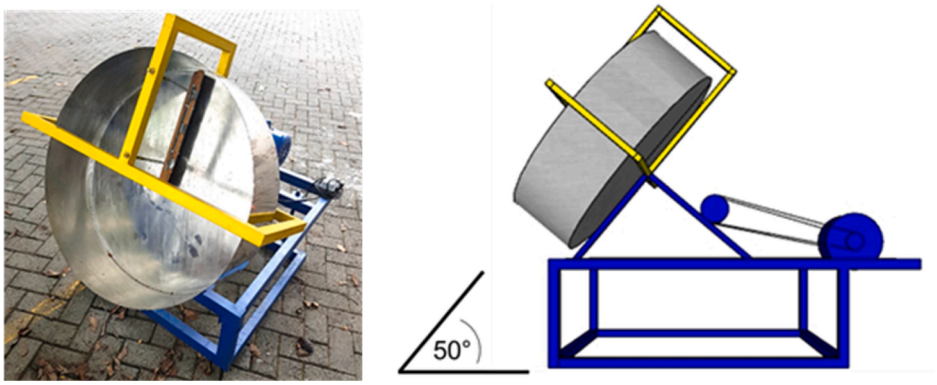

Fig. 9. Granulator pan.

Table 4
Mix design of pervious concrete (kg/m^3).

Material	Variation		
	PFBS-50	PFS-60	PFS-70
Aggregate (4.75–9.5 mm)	499	484	484
Aggregate (9.5–19 mm)	749	727	727
Portland cement	111	108	81
FA	139	162	188
BA	28	–	–
Rice husk	2.8	2.7	2.7
Water to binder ratio (w/b)	0.40	0.35	0.40

conditions.

This experimental procedure involved subjecting slab specimens to evaluate their ability to retain sediments within the pot under conditions representing a decrease in sea level in 24 h. Mud samples were obtained from coastal regions within the Wonorejo mangrove forest tourist area in Surabaya, Indonesia.

A total of 6000 g of mud was divided into two equal parts for preparation. One portion consisting of 3000 g (designated as *Sa*) was subjected to oven-drying until it reached the state of oven dryness, after which the dry weight (*So*) was determined. The remaining 3000 g of mud was placed in a plastic container, leveled on the surface, and subsequently treated with 500 mL of water, left undisturbed for 24 h to create a slurry. This slurry was poured onto the surface of the testing slab. The water and mud passing through the gaps in the slab were collected in a plastic tray, and the combined weight (*Sra*) was measured. The collected sediment was then further dried in an oven until it reached an oven-dry state (*Sro*). The calculation of sediment permeability employed Eqs. (11)–(13). These equations were employed to quantitatively analyze the sediment permeability of pervious concrete and assess its efficacy in retaining sediments within the pot structure during fluctuating sea levels, providing valuable insights into the material's performance in practical environmental scenarios. The sediment permeability assessment was conducted to quantify the extent of sediment infiltration through pervious concrete, as depicted in Fig. 13.

$$\text{Initial Sediment Content} = \frac{So}{Sa+500} \times 100\% \tag{11}$$

$$\text{Sediment Content in drained water} = \frac{Sro}{Sra} \times 100\% \tag{12}$$

$$\text{Permeated Sediment Content} = \frac{Sro}{So} \times 100\% \tag{13}$$

3.6. Concrete porosity

The formulation for calculating the total void ratio (VR) of porous concrete involves using a specimen with a diameter of 10 cm and a height of 20 cm. The ratio is determined by comparing the difference in

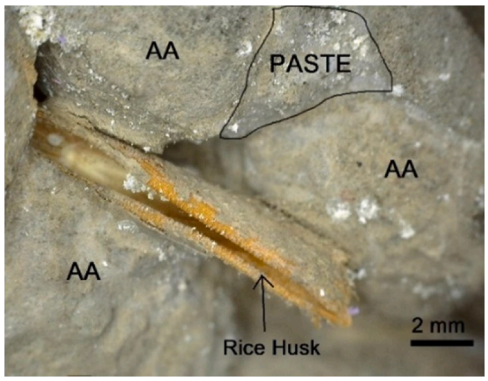

Fig. 11. A rice husk between artificial aggregate (AA) and paste.

Fig. 10. (a) Cylindrical specimens (a), (b) Slab casting, and (c) the Slab.

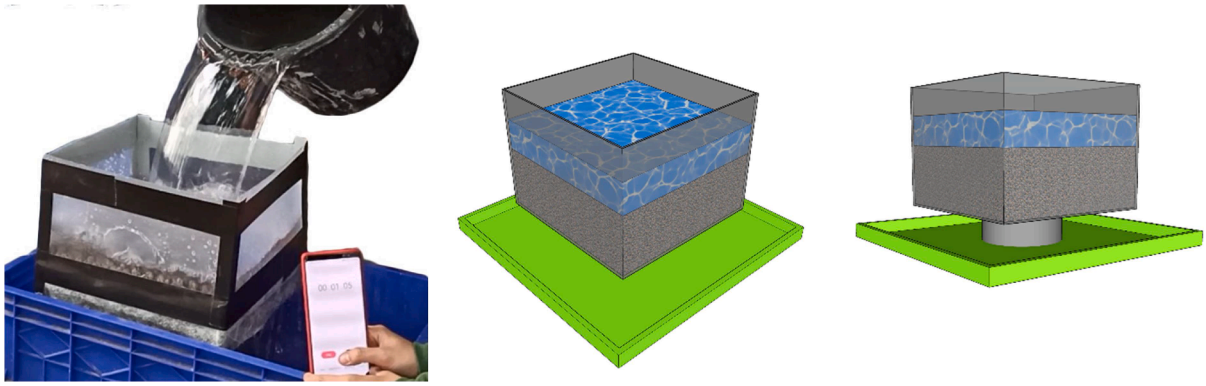

Fig. 12. Water permeability test.

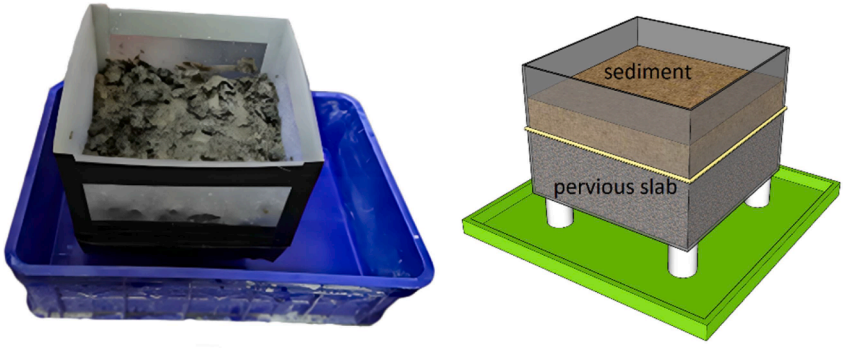

Fig. 13. Sediment permeability test.

weight of the specimen in water (W_1) with its dry weight in air-dried condition for 24 h (W_2). With the specific gravity of water (ρ_w) and the volume of the specimen (V_1), the total void is measured using Eq. (14) (Park and Tia, 2004).

$$VR = 1 - \left(\frac{W_2 - W_1}{V_1 \times \rho_w}\right) \times 100\% \quad (14)$$

4. Results and discussion

4.1. Artificial aggregates compositions, binder and mixing sequences

The selection of specific sequences and liquids in the concrete production process has a profound impact on the final characteristics of the material, including its workability, compressive strength, and mineral content. In this study, varying sequences and solvents were employed, leading to diverse outcomes. Notably, the workability of pastes, was represent by normal consistency test, utilizing NaOH 0.03 M solution as a complete replacement for 100 % of the water. It exhibited a significant increase in workability compared to pastes incorporating a combination of water and NaOH 0.03 M solution, as indicated in Table 5. This observation underscores the pivotal role of the chosen solutions and its sequence in determining the workability properties of the concrete, shedding light on the intricate relationship between material composition, mixing techniques, and the resulting mechanical characteristics of the produced concrete. The activation of FA through NaOH 0.03 M solution significantly enhanced the solubility of its particles, leading to improved workability in the resulting paste. However, this beneficial effect on workability was counterbalanced by a decrease in compressive strength. This reduction in strength occurred due to the simultaneous reaction of cement with NaOH solution, which adversely affected the overall concrete integrity.

Table 5
Workability of AFS-50 by variations of sequence.

Mixing sequences	Vicat penetration (mm)
Sequence 1	11
Sequence 2	15
Sequence 3	5
Sequence 4	15
Sequence 5	N/A

In the case of Sequence 5, the paste exhibited extremely poor workability, rendering it unsuitable for molding or workability testing. Sequence 3, despite displaying suboptimal workability, yielded the highest compressive strength. This phenomenon can be attributed to the specific proportioning in Sequence 3, where the NaOH 0.03 M solution was precisely matched with the FA content. Consequently, the FA absorbed the NaOH solution instantly, leaving no excess solution available to react with the cement. Instead, some of the water added afterward was absorbed by the FA, leaving a limited amount to react with the cement.

The compressive strengths of the paste specimens for aggregate, assessed at the 28-day mark, are illustrated in Fig. 14. A discernible trend emerged, whereby a negative correlation between FA content and compressive strength was observed. Specifically, paste specimens with lower FA content exhibited higher compressive strength values. Among the tested samples, AFS-50 consistently displayed the highest compressive strength, with AFS-40 and AFS-60 following in that order.

After considering both compressive strength and FA content, AFS-50 emerged as the most suitable choice for applications involving artificial aggregates. In the context of optimizing workability while maintaining an acceptable level of compressive strength, Sequence 2 was identified as the preferred choice. Notably, the decrease in compressive strength associated with Sequence 2 was deemed more tolerable compared to Sequence 4 as it also enhanced the ease of workmanship. Consequently, Sequence 2 was selected to produce artificial aggregates and the paste

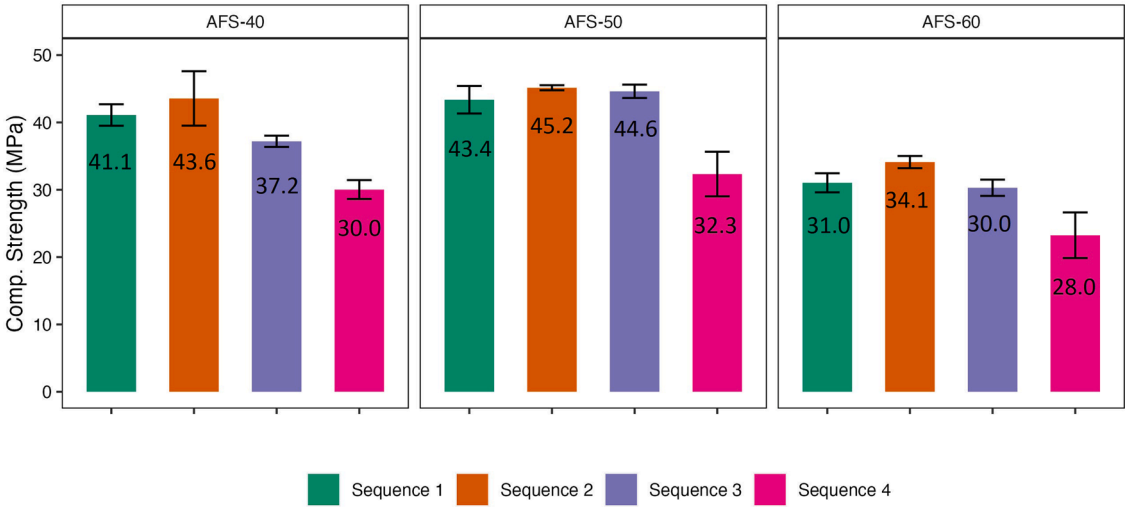

Fig. 14. Strength of paste for aggregate at 28 days.

for casting the pervious concrete, as the latter necessitates favorable workability for successful implementation.

The paste for binder formulation was selected based on its workability performance. Sequence 2 and Sequence 4, exhibiting the best flowability, were selected for testing the strength of binders PFBS-50 (containing 10 % BA and 50 % FA), PFS-60 (containing 60 % FA), and PFS-70 (containing 70 % FA). The compressive strengths of the specimens, evaluated at the 28-day mark, are depicted in Fig 15. Consistent with the results for aggregates, Sequence 2 demonstrated the most favorable performance.

The mineral composition of the 28d AFS-50 pastes for each sequence was analyzed through XRD testing. The results are presented in Fig. 16. The semi quantitative data obtained using the XRD peaks are summarized in Table 6.

The results provided valuable insights into the material's structural properties and its potential for varied applications. Significant variations in the degree of crystallinity (DOC) were observed among the samples. Although the minerals formed were similar across all sequences, their quantities varied, elucidating the pozzolanic activity that consumes portlandite ($Ca(OH)_2$) to produce calcium silicate hydrate (C-S-H) and calcium alumina silicate hydrate (C-A-S-H). The alumina source, that is rich available in FA, in the mixture containing NaOH (seq 2, 3, and 4) easily dissolved. It reacted with available calcium to form more C-A-S-H product. This mineral contributes to better mechanical and durability characteristics of pervious concrete (Nazeer et al., 2023).

Furthermore, albite was also formed as an important mineral, because of the interaction between aluminosilicate materials such as FA and alkali. Source of calcium in calcite and alumino-silica in anorthite reacted with alkali to produce albite. Albite is a type of triclinic glassy crystal, which is also a sodium aluminosilicate and considered to be a kind of N-A-S-H gel. Liquid sodium and silica from FA form the gel (Jin et al., 2021). This phenomenon was notably observed in sequences 2, 3, and 4. Albite plays a crucial role in contributing to the material's strength. Under alkaline conditions, dissolved FA facilitates the formation of alumina and silica chains with sodium ions as the positive charge carriers. The effective dispersion of FA particles in the alkali environment enables the binding of cement particles with the available water, a phenomenon demonstrated prominently in Sequence 2. This enhanced workability, as evidenced by the mixture in Sequence 2, underscores the intricate interplay between the mineral composition and the material's mechanical properties, providing valuable insights for optimizing its performance in various applications.

Fig. 17 shows the SEM analysis of 28-day specimen AFS-50 made with Sequence 2. Formation of albite and gels of calcium silicate aluminat hydrate (C-A-S-H) are found among the very dense C-S-H gels. In this study, as specific cases minerals like albite may coexist with C-A-S-H gels, especially in systems where sodium is intentionally applied. The manipulation of mineralogy in cementitious systems is a key aspect of

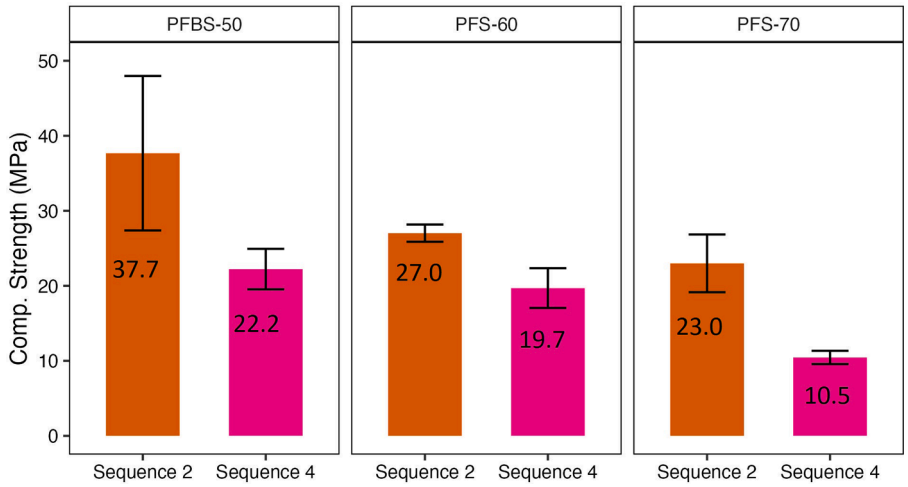

Fig. 15. Strength of paste for binder at 28 days.

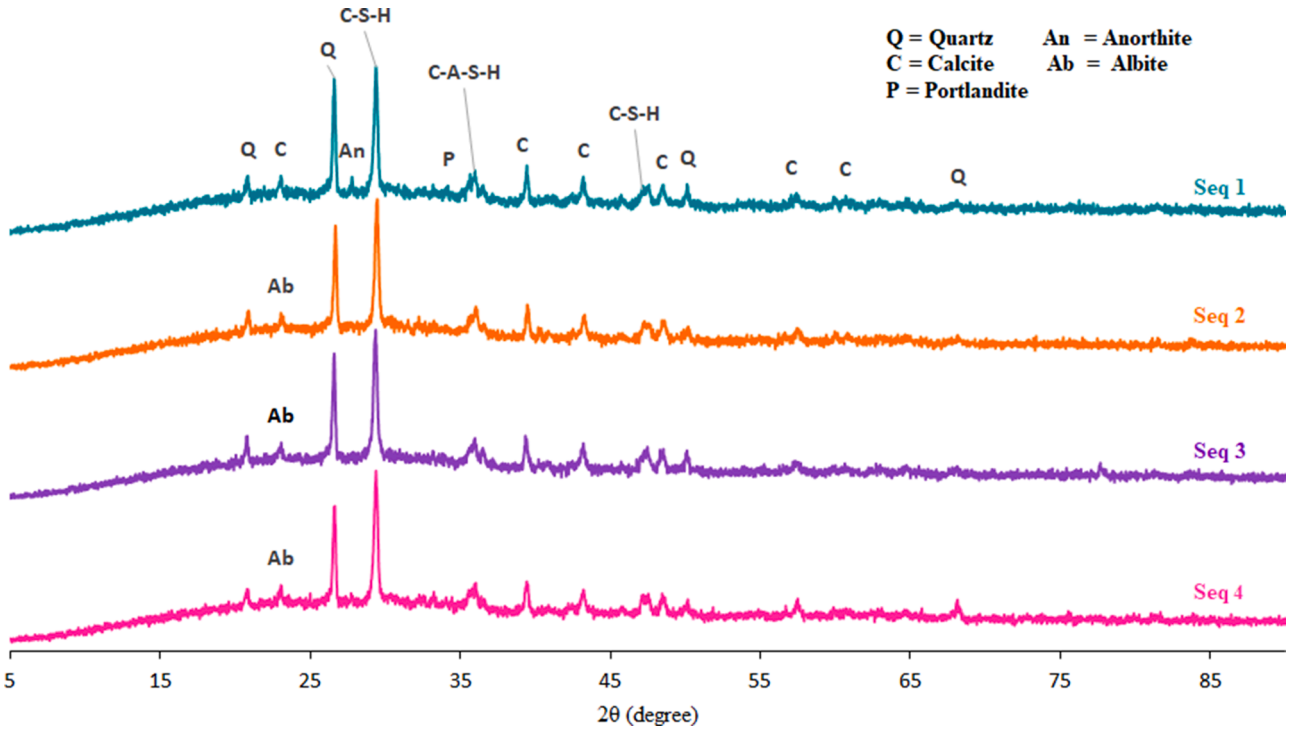

Fig. 16. XRD pattern of sampel AFS-50 with different sequences.

Table 6
Mineral content of sample AFS-50 for each sequence.

Mineral (%)	Sequence			
	1	2	3	4
C-S-H	6.8	14.0	5.9	7.4
Albite	0	2.3	1.4	1.7
C-A-S-H	1.6	2.9	2.3	2.6
Quartz	2.5	2.5	1.5	1.8
Calcite	3.4	0.5	1.5	1.6
Portlandite	0.3	0.6	0.3	0.4
Anorthite	3.8	4.6	4.2	4.0
DOC	18.3	27.3	17.1	19.4

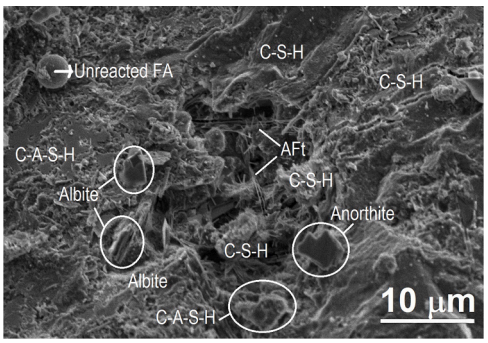

Fig. 17. SEM analysis at 5000× magnification for Sequence 2.

optimizing concrete properties for specific applications, such as improving durability, reducing environmental impact, or enhancing mechanical strength. This highlights the importance of considering the broader context and the specific goals of using HVFA in construction or other applications.

The dissolution of FA in a sodium hydroxide (NaOH) solution induces an expedited pozzolanic reaction within the FA to form N-A-S-H gels (Sun et al., 2020). Concurrently, the inherent calcite within the cement serves to augment the process of cement hydration, leading to the formation of calcium silicate hydrate (C-S-H) and calcium aluminosilicate hydrate (C-A-S-H) gels (Pratiwi et al., 2020). Consequently, in samples subjected to Sequence 2, where FA undergoes dissolution, the presence of discernible FA particles is infrequent. This configuration results in a matrix exhibiting a greater density compared to that of Sequence 1 in Fig. 18. In the latter, unreacted FA and calcite particles persist within the matrix pores, contributing to a less compacted structure. The observed disparities underscore the intricate interplay of chemical reactions and their consequential impact on the microstructure, thereby influencing the overall density of the cementitious matrix.

Observations of fly ash (FA) were conducted before and after reacting with alkali using a micro-camera at 900× magnification. In Fig. 19 (left), FA appears brownish due to the presence of iron oxide, exceeding 18 %, as indicated in Table 1. Plerosphere particles are also visible in FA, characterized by smaller spheres enclosed within larger spheres (Goodarzi and Sanei, 2009). One hour after the reaction with NaOH, depicted in Fig. 19 (right), the alkali dissolved the FA, leaving only a few remaining spherical particles. This underscores the role of alkali in

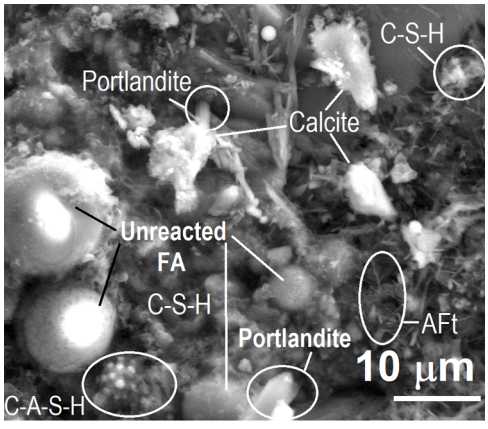

Fig. 18. SEM analysis at 5000× magnification for Sequence 1.

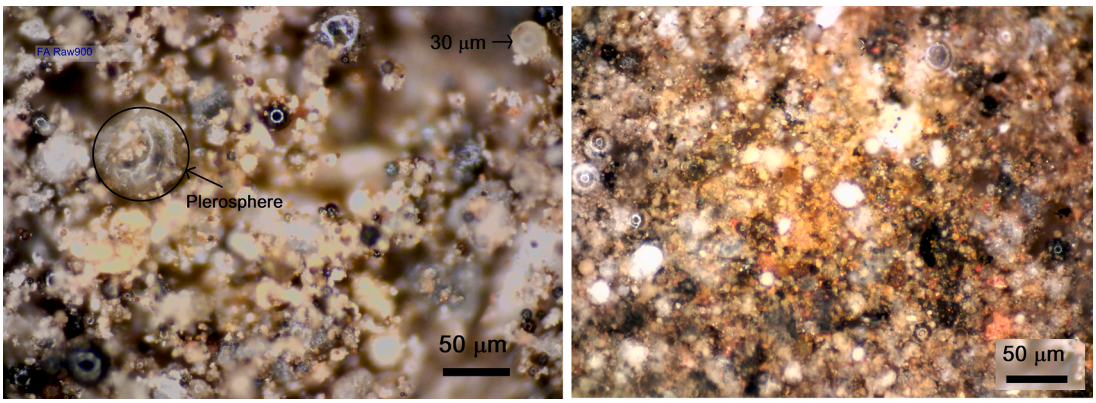

Fig. 19. FA before contact with alkali (left) after contact with alkali (right).

enhancing the workability and compressive strength of the paste.

4.2. Artificial aggregate characterization

Table 7 summarizes the test results for the artificial aggregate. Comparison of the artificial aggregates in this study with artificial aggregates from previous study using the same FA (Purnama and Ekaputri, 2021) is also provided. In our previous study, the alkali was not considered as activator for HVFA aggregate mixtures.

The manufactured artificial aggregate exhibited a dry density of 1.99 g/cm^3 and an absorption rate of 9.29 %. These characteristics align with the specifications outlined in ASTM (C127, 2015) for coarse aggregates, highlighting the successful replication of the desired physical properties. This uniformity in density and absorption underscores the precision and efficacy of the production process, ensuring the artificial aggregate's suitability for applications in various construction and engineering contexts. However, the absorption rate of artificial aggregate was relatively high, which was 9.29 %. In ACI 221 R, the general absorption rate of natural aggregate is 0.2 % - 4 % (ACI, 1996). The artificial aggregates under examination exhibited a total porosity of 16.32 %, primarily dominated by open porosity at a rate of 13.48 %. The remaining portion of the porosity was attributed to closed pores. Notably, a direct correlation between the FA content and the size of porous diameter was observed, indicating that higher FA content led to the generation of larger pores (Zhao et al., 2018). The substantial open porosity significantly influenced the absorption rate, as open pores readily absorbed and evaporated water. To mitigate this effect, the aggregates in this study were subjected to oven-dry condition to minimize the residual water content. It is worth noting that open porosity plays a crucial role in strengthening the interfacial zone between the binder and aggregate (Frankovič et al., 2017).

The presence of calcium silicate hydrate (C-S-H) as a hydration product further contributed to filling the pores, enhancing the aggregate's density (Mehta et al., 2020). The artificial aggregates were subjected to testing at an age of 182 days, allowing sufficient time for the pores to be partially filled with CSH. Comparative analysis, as presented in Table 7, revealed that the artificial aggregates in this study exhibited a lower porosity rate despite having an identical composition of FA and Portland cement when compared to previous studies using Sequence 1 (Purnama and Ekaputri, 2021).

Table 7
Comparison of aggregate's oven dry density and absorption.

Artificial aggregate properties	This study	Previous research (Purnama and Ekaputri, 2021)
Oven dry density (gr/cm^3)	1.99	1.59
Absorption (%)	9.29	23
Total porosity (%)	16.32	27.05
Open porosity (%)	13.48	24.15
Closed porosity (%)	2.84	2.9
Abration rate (%) Size 4.75 – 9.50 mm	27.49	N/A
Abration rate (%) Size 9.50–19.00 mm	31.51	35.4

According to ASTM (C33, 2018), the maximum allowable aggregate abrasion for concrete is specified at 50 %. In this study, the artificial aggregate abrasion rates were measured at 27.48 % for diameters ranging from 4.75 mm to 9.5 mm and 32.56 % for diameters ranging from 9.5 mm to 19 mm. The abrasion of bigger diameter is greater because in its production, granulation speed has an impact to the paste compaction. With the same speed, smaller aggregates scrolled faster on the granulator pan resulting in denser compaction. However, these abrasion rates fell well within the specified limits, demonstrating the suitability of the artificial aggregates for concrete applications. This outcome underscores the superior abrasion resistance exhibited by the artificial aggregates developed in this study, highlighting their potential for enhancing the durability and longevity of concrete structures while conforming to industry standards.

4.3. Pervious concrete strength

The testing results of pervious concrete compression tests are illustrated in Fig. 20. Among the various compositions, PFS-60 exhibited the highest compressive strength at both 28 and 56 days, surpassing PFBS-50 and PFS-70 in performance as it has lower water to binder ratio of 0.35 compared to other ratio of 0.4. It was also reported that the compressive strength, splitting tensile and the flexural strength of pervious concrete tended to decrease as the water content increase (Park et al., 2022). As Notably, PFS-60 achieved the target compressive strength of 3–5 MPa, indicating its suitability for the intended applications. Beside the water content, it was observed that an increase in FA content from 60 % (PFBS-50) to 70 % (PFS-70) with the same water content, corresponded to a decrease in compressive strength. However, all samples exhibited a significant improvement in compressive strength at the age of 56 days. This phenomenon aligns with the behavior of HVFA concrete, which initially displays lower compressive strength but gradually increases over time and superior durability in marine area (Andharia et al., 2023; Madhavi et al., 2014). These findings underscore the influence of the curing duration and the unique characteristics of the pervious concrete mixtures, offering valuable insights into the material's mechanical properties and long-term performance (Khankhaje et al., 2023). For later ages, specifically at 120 days, the strength development of pervious concrete containing FA typically shows no significant difference compared to the strength observed at 56 days (Nazeer et al., 2023).

Compressive strength test for concrete PFS-60 and PFBS-50 without fiber was conducted to identify the effect of rice husk as the natural

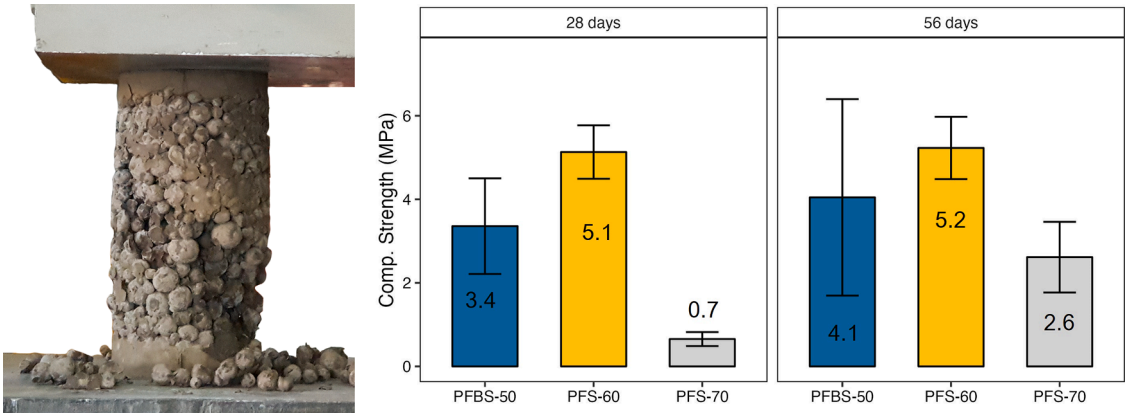

Fig. 20. Pervious concrete compressive strength.

fiber. The compressive strength of non-fiber PFBS-50 and PFS-60 at 28 days is reported as 3.2 MPa and 4.6 MPa, respectively. It was observed that the inclusion of fibers has a positive impact, contributing to an increase in compressive strength of up to 10 %. In general, it has more effect to the tensile strength (Ekaputri et al., 2021).

The strength in Fig. 20 is correlated with the density of the pervious concrete where PFBS-50, PFS-60 and PFS-70 had a density of 1710 kg/m^3, 1750 kg/m^3, and 1580 kg/m^3 respectively. The void ratio (VR) of PFBS-50, PFS-60 and PFS-70 were 19.2 %, 17.2 % and 25.5 %, respectively. Comparing with previous study, this study has a good agreement. It was reported that porous concrete with density in the range of 1638–1875 kg/m^3 had a linear relation with its compressive strength of 1.06–6.95 MPa (Ibrahim et al., 2014). Void ratio of concrete also has a linear relation with the strength. Previous study showed that concrete with VR in the range of 18–30 % has compressive strength of 1.8–9.4 MPa (Furkan Ozel et al., 2022).

To assess the influence of seawater exposure in tidal areas, cylindrical test specimens for variation PFBS-50 and PFBS-60, after the of aged 28 days, were positioned near mangroves subjected to tidal and receding waves for 240 days. The compressive strength test results is presented in Fig. 21 where the initial compressive strength at 0 days of curing in the 28-day compressive strength in Fig. 20. The results show minimal change in compressive strength in seawater exposure. Notably, there is an increase in compressive strength from 30 days to 56 days of specimens exposure in the tidal area, with subsequent limited variation in compressive strength thereafter.

The application of aggregates in this study exhibited an unevenly distributed gradation, as depicted in Fig. 22. During the compression testing process, aggregates that were strongly coated with binder tended to fracture and split. Conversely, aggregates with a minimal binder coating were more prone to detachment from the concrete matrix without undergoing splitting. This observation highlights the critical role of binder distribution in influencing the structural behavior of the aggregates within the concrete matrix, shedding light on the mechanisms governing the interaction between the binder and aggregates during compression testing.

4.4. *Water and sediment permeability*

The test results, summarized in Table 8, revealed the high water permeability rates across all pervious concrete variations. Each sample demonstrated efficient water passage, allowing the passage of up to 10 liters of water through the slab specimens in less than 10 s.

This heightened permeability was attributed to the gap-graded gradation of the aggregates and inadequate planning. Controlling aggregate sizes is proven to ensure the void ratio and permeability in

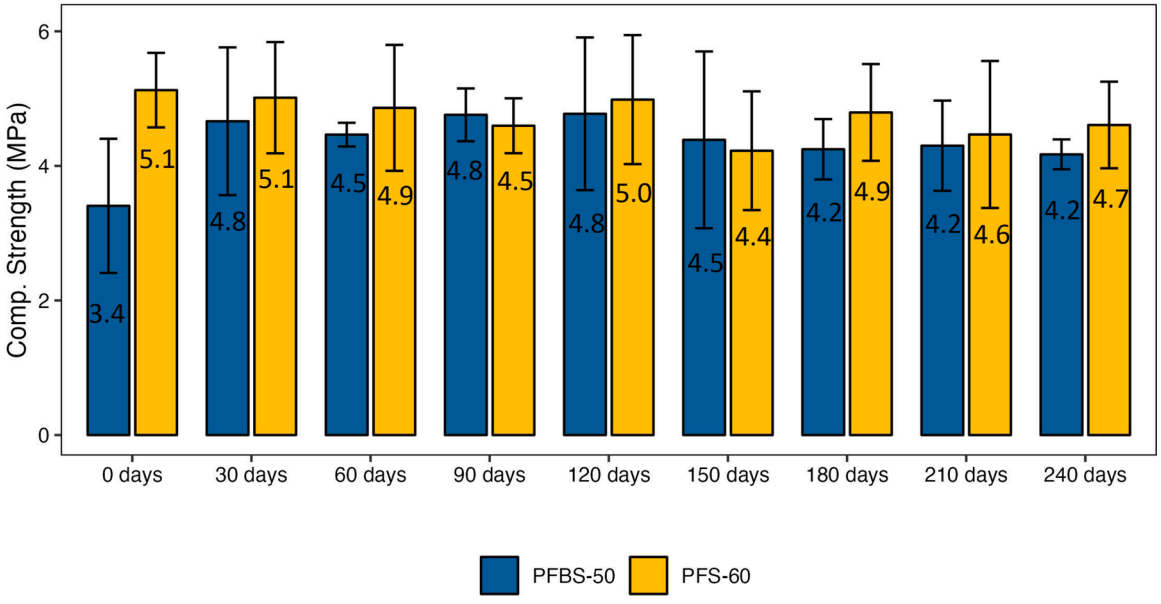

Fig. 21. Compressive strength in marine area for 8 months.

Fig. 22. Crushed pervious concrete.

Table 8
Water and sediment permeability.

Property	Sample		
	PFBS-50	PFS-60	PFS-70
Water permeability (liter/m^2/minute)	966	694	1182
Initial sediment content (%)	67.0	60.0	63.5
Sediment content in drained water (%)	0	0	0
Permeated sediment content (%)	0	0	0

mixes by addressing the increased porous nature of the concrete matrix due to a lack of fine aggregates (Bright Singh et al., 2023). Effective water permeability necessitates meticulous planning and a well-executed design to minimize such high flow rates. Furthermore, the sediment permeability test demonstrated that all pervious concrete variations successfully retained sediment within the pot structure. In essence, the application of concrete as a container for mangrove saplings does not impede seawater circulation. Even during a decrease in sea level, the sediment remains securely contained within the pot, confirming the efficacy of the pervious concrete design for its intended purpose

4.5. Required strength of pervious concrete

The tensile strength of pervious concrete is generally assumed to be 5–6 % of its compressive strength . However, for non-structural concrete, this value is typically set between 4 and 5 % of the compressive strength (Sherwani et al., 2021). In this study, a conservative estimate of 1.5 % was considered for the tensile strength in correlation with the compressive strength, as outlined in Table 9.

Among the three variations, PBFS-50 and PFS-60 emerged as variants capable of withstanding both internal and external pressures in terms of tensile strength, satisfying the necessary criteria. To elucidate, the target compressive strength range of 3–5 MPa was calculated, taking into account both the internal forces of 0.04 MPa, induced by the sediment and the external wave forces specifically relevant to the East Java area, Indonesia. For broader applicability in different territories, it is advisable to conduct further studies tailored to the unique environmental factors and conditions of each specific area. Nevertheless, the outcomes

Table 9
Correlation between tensile strength and compressive strength.

Sample	Compressive strength (MPa)	Tensile strength (MPa)
PFBS-50	3.4	0.05
PFS-60	5.1	0.08
PFS-70	0.7	0.01

of this study serve as a foundational reference, providing valuable insights and a methodological framework that can inform subsequent research endeavors aimed at developing pervious concrete pot structures for mangrove saplings in diverse geographical locations.

5. Conclusions

These conclusions provide essential insights into the properties and applications of the materials and structures studied, offering valuable information for their effective utilization in various engineering and environmental contexts. This study yields several key conclusions:

1. The utilization of NaOH 0.03 M solution to replace water is recommended for HVFA mixture with a certain blending sequence. As outlined in sequences 2 and 4, the mixture resulted in a notable increase in workability, reaching up to 37 % of the normal paste workability. In contrast, the partial replacement of water with NaOH 0.03 M solution, as exemplified by sequences 3 and 5, led to a decrease in workability by as much as 5 %. Given its superior workability, good mechanical property, and ease of application, Sequence 2 emerged as the preferred choice to produce artificial aggregates and pervious concrete.
2. Due to the substantial presence of FA, calcium-aluminum-silicate-hydrate (CASH) was found as an additional product in the HVFA mixture, alongside calcium-silicate-hydrate (CSH). Notably, the utilization of a low alkali agent, such as NaOH 0.03 M, induced a mineralogical transformation from calcite to albite. This transformation holds significance in augmenting the volumetric density of the hydration products, thereby impacting the material's structural properties.
3. The production of HVFA artificial aggregate with FA content of 50 % from the total material weight, manufactured using a granulator, resulted in suboptimal compaction. This, in turn, led to a high porosity, primarily characterized by open porosity, which lightened the aggregate and elevated its absorption rate. Furthermore, the prevalence of open porosity facilitated the rapid absorption and evaporation of water. Despite these characteristics, the abrasion rate of the HVFA artificial aggregate remained within the specifications required for aggregate used in concrete.
4. The paste compositions from PFS-60 and PFBS-50, employing AFS-50 aggregates, emerged as the most suitable choice for application in pervious concrete pot structures. This composition successfully achieved the target compressive strength range of 3–5 MPa. Furthermore, the pervious concrete exhibited the capacity to facilitate water passage while securely retaining sediment within the pot, making it a practical choice for the intended application, as the protection for mangrove saplings.
5. Despite its relatively modest contribution to increasing compressive strength, it is recommended to incorporate rice husks at a rate of 1 % of the weight of the cementitious material. This natural material can be relied upon to enhance the compressive strength of pervious concrete, with an achievable maximum increase of up to 10 %. This is expected to be advantageous in field applications, particularly during the transportation and placement of pot segments from land to mangrove areas.

While the pervious concrete in this study met its planned targets, there remains a need for further research into implementing a mangrove conservation project. This involves conducting trials with mangrove saplings in real locations using permeable pots. It is crucial to understand the interaction between the mechanical properties of the pot and its durability in the sediment environment of tidal areas. The results obtained from exposing the specimens in the tidal area were insufficient to fully describe the pot's durability as per its intended function, which was designed to last for 3–4 years. Moreover, considering the prevalence of sulfate content in mangrove areas, its potential influence on pots may

outweigh that of chloride ions attack, which could potentially lead to the breakdown of cement hydration gels bonds.

CRediT authorship contribution statement

Januarti Jaya Ekaputri: Conceptualization, Data curation, Formal analysis, Funding acquisition, Investigation, Methodology, Supervision, Writing – original draft, Writing – review & editing. **Xevna De Elshinta Arellsya Ruitan:** Formal analysis, Methodology, Project administration, Software, Visualization, Writing – original draft. **Himawan Tri Bayu Murti Petrus:** Data curation, Investigation, Resources. **Martin Anda:** Formal analysis, Investigation. **Liliek Harmianto Purbawinasta:** Data curation, Formal analysis, Resources. **Irwanda Laory:** Data curation, Formal analysis, Investigation. **Davin H.E. Setiamarga:** Conceptualization, Data curation, Investigation, Methodology, Supervision, Writing – original draft. **Nobuhiro Chijiwa:** Investigation, Methodology, Validation. **Chikako Fujiyama:** Conceptualization, Investigation, Methodology, Supervision, Visualization.

Declaration of competing interest

The authors declare the following financial interests/personal relationships which may be considered as potential competing interests: Januarti Jaya Ekaputri reports financial support was provided by Sepuluh Nopember Institute of Technology. Januarti Jaya Ekaputri reports a relationship with Ministry of Education Culture Research and Technology that includes: funding grants. If there are other authors, they declare that they have no known competing financial interests or personal relationships that could have appeared to influence the work reported in this paper.

Data availability

Data will be made available on request.

Acknowledgement

The authors express their gratitude for the financial support provided by Institut Teknologi Sepuluh Nopember for this work, through the project scheme of the Publication Writing and IPR Incentive Program (PPHKI). Additionally, part of the testing conducted by JJE received support from the Ministry of Education, Culture, Research, and Technology of the Republic of Indonesia through Penelitian Fundamental-Reguler, with the contract no. 1943/PKS/ITS/2023.

References

ACI, R., 1996. Guide For Use of Normal Weight and Heavyweight Aggregates in Concrete. American Concrete Institute.
ACI, R., 2010. Report On Pervious Concrete. American Concrete Institute.
Adamu, M., Ayeni, K.O., Haruna, S.I., Ibrahim Mansour, Y.E.-H., Haruna, S., 2021. Durability performance of pervious concrete containing rice husk ash and calcium carbide: a response surface methodology approach. Case Stud. Constr. Mater. 14.
Adresi, M., Yamani, A., Karimaei Tabarestani, M., Rooholamini, H., 2023. A comprehensive review on pervious concrete. Constr. Build. Mater. 407.
Akram, H., Hussain, S., Mazumdar, P., Chua, K.O., Butt, T.E., Harikrishna, J.A., 2023. Mangrove health: a review of functions, threats, and challenges associated with mangrove management practices. Forests. 14 (9).
Akturk, B., Yuzer, N., Kabay, N., 2016. Usability of raw rice husk instead of polypropylene fibers in high-strength concrete under high temperature. J. Mater. Civil Eng. 28 (1).
Al Biajawi, M.I., Embong, R., Muthusamy, K., Ismail, N., Obianyo, I.I., 2022. Recycled coal bottom ash as sustainable materials for cement replacement in cementitious composites: a review. Constr. Build. Mater. 338.
Andharia, B.R., Dhar, S., Thakkar, S., Dave, U., Patel, K., 2023. Sustainable high volume fly ash concrete with recycled C&D waste and dredged marine sand. In: Materials Today: Proceedings.
Arenas, C., Leiva, C., Vilches, L.F., Cifuentes, H., Rodríguez-Galán, M., 2015. Technical specifications for highway noise barriers made of coal bottom ash-based sound absorbing concrete. Constr. Build. Mater. 95, 585–591.
Aydin, E., Arel, H.Ş., 2017. Characterization of high-volume fly-ash cement pastes for sustainable construction applications. Constr. Build. Mater. 157, 96–107.
Bright Singh, S., Murugan, M., Chellapandian, M., Dixit, S., Bansal, S., Sunil Kumar Reddy, K., Gupta, M., Maksudovna Vafaeva, K., 2023. Effect of fly ash addition on the mechanical properties of pervious concrete. In: Materials Today: Proceedings.
C33, A., 2018. Standard Specification for Concrete Aggregates. ASTM International, West Conshohocken, PA.
C127, A., 2015. Standard Test Method For Relative Density (Specific Gravity) and Absorption of Coarse Aggregate. ASTM International, West Conshohocken, PA.
C187, A., 2016. Standard Test Method For Amount of Water Required For Normal Consistency of Hydraulic Cement Paste. ASTM International, PA, United States.
C595, A., 2020. Standard Specification for Blended Hydraulic Cements. ASTM International, West Conshohocken, PA.
C618, A., 2019. Standard Specification for Coal Fly Ash and Raw or Calcined Natural Pozzolan for Use in Concrete. ASTM International, West Conshohocken, PA.
C642, A., 2013. Standard Test Method For Density, Absorption, and Voids in Hardened Concrete. ASTM International, West Conshohocken, PA.
Chabi, E., Lecomte, A., Adjovi, E.C., Dieye, A., Merlin, A., 2018. Mix design method for plant aggregates concrete: example of the rice husk. Constr. Build. Mater. 174, 233–243.
Chen, L., Chen, Z., Xie, Z., Wei, L., Hua, J., Huang, L., Yap, P.-S., 2023. Recent developments on natural fiber concrete: a review of properties, sustainability, applications, barriers, and opportunities. Develop. Built Environ. 16.
Cooke, S.J., Bergman, J.N., Nyboer, E.A., Reid, A.J., Gallagher, A.J., Hammerschlag, N., Van de Riet, K., Vermaire, J.C., 2020. Overcoming the concrete conquest of aquatic ecosystems. Biol. Conserv. 247.
Darmansyah, D., You, S.-J., Wang, Y.-F., 2023. Advancements of coal fly ash and its prospective implications for sustainable materials in Southeast Asian countries: a review. Renew. Sustain. Energy Rev. 188.
Doumongue, B., Limam, K.Y.M.X., Dany, A., Mastouri, H., Bahi, H., El Bouazouli, A., 2023. Analysis of rice husk concrete samples observed by scanning electron microscopy. In: Materials Today: Proceedings, 72, pp. 3850–3856.
E1-16, E.B, 2016. Aggregates For Concrete, ACI. American Concrete Institute, pp. 1–26.
Ekaputri, J.J., Fujiyama, C., Chijiwa, N., Ho, T.D., Nguyen, H.T., 2021. Improving geopolymer characteristics with addition of poly-vinyl alcohol (PVA) fibers. Civil Eng. Dimen. 23 (1), 28–34.
Faturachman, A., Raharjo, P., 2003. The carrying capacity of seabed sediment in the waters of Cirebon Harbor and its adjacent regions. Jurnal Geologi Kelautan 1 (1), 15–29.
Frankovič, A., Bokan Bosiljkov, V., Ducman, V., 2017. Lightweight aggregates made from fly ash using the cold-bond process and their use in lightweight concrete. Materiali in tehnologije 51 (2), 267–274.
Furkan Ozel, B., Sakallı, Ş., Şahin, Y., 2022. The effects of aggregate and fiber characteristics on the properties of pervious concrete. Constr. Build. Mater. 356.
Goodarzi, F., Sanei, H., 2009. Plerosphere and its role in reduction of emitted fine fly ash particles from pulverized coal-fired power plants. Fuel 88 (2), 382–386.
Gupta, N., Gedam, V.V., Moghe, C., Labhasetwar, P., 2019. Comparative assessment of batch and column leaching studies for heavy metals release from coal fly ash bricks and clay bricks. Environ. Technol. Innov. 16.
Gupta, V., Siddique, S., Chaudhary, S., 2021. Optimum mixing sequence and moisture content for hydrated lime fly ash bricks. J. Clean. Prod. 285.
Ibrahim, A., Mahmoud, E., Yamin, M., Patibandla, V.C., 2014. Experimental study on Portland cement pervious concrete mechanical and hydrological properties. Constr. Build. Mater. 50, 524–529.
Jin, L., Huang, G., Li, Y., Zhang, X., Ji, Y., Xu, Z., 2021. Positive influence of liquid sodium silicate on the setting time, polymerization, and strength development mechanism of MSWI bottom ash alkali-activated mortars. Materials. (Basel) 14 (8).
Khankhaje, E., Kim, T., Jang, H., Kim, C.-S., Kim, J., Rafieizonooz, M., 2023. Properties of pervious concrete incorporating fly ash as partial replacement of cement: a review. Develop. Built Environ. 14.
Lawala, A.Q.T., Ninsiimaa, E., Odebiyib, O.S., Hassanc, A.S., Oyagbola, I.A., Onu, P., Yusuf, D.A., Japyem, E., 2019. Effect of unburnt rice husk on the properties of concrete. In: 2nd International Conference on Sustainable Materials Processing and Manufacturing (SMPM 2019). Procedia Manufacturing, pp. 635–640.
Laxman Kudva, P., Nayak, G., Shetty, K.K., Sugandhini, H.K., 2022. A sustainable approach to designing high volume fly ash concretes. In: Materials Today: Proceedings, 65, pp. 1138–1145.
Lee, B.J., Prabhu, G.G., Lee, B.C., Kim, Y.Y., 2016. Eco-friendly porous concrete using bottom ash aggregate for marine ranch application. Waste Manage. Res. J. Int. Solid Wastes Public Cleans. Assoc., ISWA 34 (3), 214–224.
Li, Q., Zhao, Y., Chen, H., Zhao, P., Hou, P., Cheng, X., Xie, N., 2021. Effect of waste corn stalk ash on the early-age strength development of fly ash/cement composite. Constr. Build. Mater. 303.
Liu, J., Xie, X., Li, L., 2022. Experimental study on mechanical properties and durability of grafted nano-SiO2 modified rice straw fiber reinforced concrete. Constr. Build. Mater. 347.
Liu, J., Zhao, W., Li, L., 2023. Effects of Nano-SiO2 grafting on improving the interfacial and mechanical properties of concrete with rice straw fibers. Constr. Build. Mater. 398.
Lo, F.-C., Lee, M.-G., Lo, S.-L., 2021. Effect of coal ash and rice husk ash partial replacement in ordinary Portland cement on pervious concrete. Constr. Build. Mater. 286.
Luo, W., Li, B., Yang, G., Xu, M., Pang, C., Kow, K.-W., Wu, T., 2024. Utilisation of electrolytic manganese residue as a sulphate activator in producing concrete blocks with high-volume fly ash. J. Clean. Prod. 434.

Madhavi, T.C., Raju, L.S., Mathur, D., 2014. Durabilty and strength properties of high volume fly ash concrete. J. Civil Eng. Res. 4 (2A), 7–11.
Mangi, S.A., Wan Ibrahim, M.H., Jamaluddin, N., Arshad, M.F., Shahidan, S., 2019. Performances of concrete containing coal bottom ash with different fineness as a supplementary cementitious material exposed to seawater. Eng. Sci. Technol. Int. J. 22 (3), 929–938.
Mehta, A., Siddique, R., Ozbakkaloglu, T., Uddin Ahmed Shaikh, F., Belarbi, R., 2020. Fly ash and ground granulated blast furnace slag-based alkali-activated concrete: mechanical, transport and microstructural properties. Constr. Build. Mater. 257.
Montgomery, J.M., Bryan, K.R., Coco, G., 2022. The role of mangroves in coastal flood protection: the importance of channelization. Cont. Shelf Res. 243.
Morris, R.L., Fest, B., Stokes, D., Jenkins, C., Swearer, S.E., 2023. The coastal protection and blue carbon benefits of hybrid mangrove living shorelines. J. Environ. Manage. 331, 117310.
Nazeer, M., Kapoor, K., Singh, S.P., 2023. Strength, durability and microstructural investigations on pervious concrete made with fly ash and silica fume as supplementary cementitious materials. J. Build. Eng. 69.
Nguyen, T.P., Luom, T.T., Parnell, K.E., 2017. Mangrove transplantation in Brebes Regency, Indonesia: lessons and recommendations. Ocean Coast. Manag. 149, 12–21.
Palomo, A., Fernández-Jiménez, A., Kovalchuk, G., Ordoñez, L.M., Naranjo, M.C., 2007. Opc-fly ash cementitious systems: study of gel binders produced during alkaline hydration. J. Mater. Sci. 42 (9), 2958–2966.
Park, J.H., Jeong, S.T., Bui, Q.T., Yang, I.H., 2022. Strength and permeability properties of pervious concrete containing coal bottom ash aggregates. Materials. (Basel) 15 (21).
Park, S.-B., Tia, M., 2004. An experimental study on the water-purification properties of porous concrete. Cem. Concr. Res. 34 (2), 177–184.
Park, S.B., Jang, Y.I., Lee, J., Lee, B.J., 2009. An experimental study on the hazard assessment and mechanical properties of porous concrete utilizing coal bottom ash coarse aggregate in Korea. J. Hazard. Mater. 166 (1), 348–355.
Parkinson, R.W., Wdowinski, S., 2022. Accelerating sea-level rise and the fate of mangrove plant communities in South Florida, U.S.A. Geomorphology 412.
Pratiwi, W.D., Fansuri, H., Ekaputri, J.J., Triwulan, 2017. Effect of activators on strength of hybrid alkaline cement. In: IOP Conference Series: Materials Science and Engineering, p. 196.
Pratiwi, W.D., Triwulan, Ekaputri, J.J., Fansuri, H., 2020. Combination of precipitated-calcium carbonate substitution and dilute-alkali fly ash treatment in a very high-volume fly ash cement paste. Constr. Build. Mater. 234.
Promsawat, P., Chatveera, B., Sua-iam, G., Makul, N., 2020. Properties of self-compacting concrete prepared with ternary Portland cement-high volume fly ash-calcium carbonate blends. Case Stud. Constr. Mater. 13.
Purnama, A.C., Ekaputri, J.J., 2021. Fly ash utilization as the artificial aggregates in concrete mixture. Journal Manajemen Aset Infrastruktur & Fasilitas 5 (2), 107–120.
Qi, Y., Wang, Q., Luo, H., He, P., Deng, Q., 2023. Effects of calcium sulfate as activator on mechanical properties of PVA fiber reinforced cementitious composites with high-volume fly ash. Powder Technol. 430.
Rafieizonooz, M., Mirza, J., Salim, M.R., Hussin, M.W., Khankhaje, E., 2016. Investigation of coal bottom ash and fly ash in concrete as replacement for sand and cement. Constr. Build. Mater. 116, 15–24.
Rupesh, Arvinda, Reddy, R., 2015. Utilization of fly ash aggregates in pervious concrete. Int. J. Eng. Res. Technol. (IJERT) 4 (8), 449–452.
Sabdaningsih, A., Adyasari, D., Suryanti, S., Febrianto, S., Eshananda, Y., 2023. Environmental legacy of aquaculture and industrial activities in mangrove ecosystems. J. Sea Res. 196.
Salas_Montoya, A., Chung, C.-W., Mira_Rada, B.E., 2023. Interaction effect of recycled aggregate type, moisture state, and mixing process on the properties of high-performance concretes. Case Stud. Constr. Mater. 18.
Sam, K., Zabbey, N., Gbaa, N.D., Ezurike, J.C., Okoro, C.M., 2023. Towards a framework for mangrove restoration and conservation in Nigeria. Reg. Stud. Mar. Sci. 66.
Shah, H., Ramesh, R., 2022. Development-aligned mangrove conservation strategy for enhanced blue economy: a successful model from Gujarat, India. Estuar. Coast. Shelf Sci. 274.
Shanmugan, S., Deepak, V., Nagaraj, J., Jangir, D., Viyagula Jegan, S., Palani, S., 2020. Enhancing the use of coal-fly ash in coarse aggregates concrete. In: Materials Today: Proceedings, 30, pp. 174–182.
Sherwani, A.F.H., Faraj, R., Younis, K.H., Daraei, A., 2021. Strength, abrasion resistance and permeability of artificial fly-ash aggregate pervious concrete. Case Stud. Constr. Mater. 14.
Sievers, M., Brown, C.J., McGowan, J., Turschwell, M.P., Buelow, C.A., Holgate, B., Pearson, R.M., Adame, M.F., Andradi-Brown, D.A., Arnell, A., Mackey, B.G., Ermgassen, P., Gosling, J., McOwen, C.J., Worthington, T.A., Connolly, R.M., 2023. Co-occurrence of biodiversity, carbon storage, coastal protection, and fish and invertebrate production to inform global mangrove conservation planning. Sci. Total. Environ. 904, 166357.
Singh, M., Siddique, R., 2016. Effect of coal bottom ash as partial replacement of sand on workability and strength properties of concrete. J. Clean. Prod. 112, 620–630.
Singh, S., 2021. Examination of fibrous concrete casted using rural materials. Materials Today: Proceedings 37, 3593–3596.
Stankovic, M., Mishra, A.K., Rahayu, Y.P., Lefcheck, J., Murdiyarso, D., Friess, D.A., Corkalo, M., Vukovic, T., Vanderklift, M.A., Farooq, S.H., Gaitan-Espitia, J.D., Prathep, A., 2023. Blue carbon assessments of seagrass and mangrove ecosystems in South and Southeast Asia: current progress and knowledge gaps. Sci. Total. Environ. 904, 166618.
Strain, E.M.A., Kompas, T., Boxshall, A., Kelvin, J., Swearer, S., Morris, R.L., 2022. Assessing the coastal protection services of natural mangrove forests and artificial rock revetments. Ecosyst. Serv. 55.
Sun, G., Tang, Q., Zhang, J., Liu, Z., 2020. Early activation of high volume fly ash by ternary activator and its activation mechanism. J. Environ. Manage 267, 110638.
Takagi, H., 2023. Survival of young planted mangroves in a calm bay environment during a tropical cyclone. Nature-Based Sol. 4.
Tamanna, K., Raman, S.N., Jamil, M., Hamid, R., 2023. Coal bottom ash as supplementary material for sustainable construction: a comprehensive review. Constr. Build. Mater. 389.
Tijani, M.A., Ajagbe, W.O., Agbede, O.A., 2022. Recycling sorghum husk and palm kernel shell wastes for pervious concrete production. J. Clean. Prod. 380.
Tuan, T.Q., Luan, M.T., Cuong, L.N., 2022. Laboratory study of wave damping by porous breakwaters on mangrove mudflats in the Mekong River Delta. Ocean Eng. 258.
Ul Rehman, M., Rashid, K., Ul Haq, E., Hussain, M., Shehzad, N., 2020. Physico-mechanical performance and durability of artificial lightweight aggregates synthesized by cementing and geopolymerization. Constr. Build. Mater. 232.
van Hespen, R., Hu, Z., Borsje, B., De Dominicis, M., Friess, D.A., Jevrejeva, S., Kleinhans, M.G., Maza, M., van Bijsterveldt, C.E.J., Van der Stocken, T., van Wesenbeeck, B., Xie, D., Bouma, T.J., 2023. Mangrove forests as a nature-based solution for coastal flood protection: biophysical and ecological considerations. Water Sci. Eng. 16 (1), 1–13.
Vieira, G.L., Schiavon, J.Z., Borges, P.M., da Silva, S.R., de Oliveira Andrade, J.J., 2020. influence of recycled aggregate replacement and fly ash content in performance of pervious concrete mixtures. J. Clean. Prod. 271.
Wilińska, I., 2023. Investigation of physicochemical processes taking place in chemically activated very high volume fly ash mixtures. Constr. Build. Mater. 406.
Wu, J., Wong, H.S., Zhang, H., Yin, Q., Jing, H., Ma, D., 2024. Improvement of cemented rockfill by premixing low-alkalinity activator and fly ash for recycling gangue and partially replacing cement. Cem. Concr. Compos. 145.
Yuliana, H., Karyawan, I.D.M.A., Murtiadi, S., Ekaputri, J.J., Ahyudanari, E., 2019. The effect of slope granulator on the characteristic of artificial geopolymer aggregate used in pavement. J. Eng. Sci. Technol. 14 (3), 1466–1481. No. 3 (2019) 1466-1481.
Zhao, H., Qin, X., Liu, J., Zhou, L., Tian, Q., Wang, P., 2018. Pore structure characterization of early-age cement pastes blended with high-volume fly ash. Constr. Build. Mater. 189, 934–946.